Optical characterization of coupled resonator slow-light rib waveguides

Jeremy Goeckeritz and Steve Blair*

Department of Electrical and Computer Engineering, University of Utah, 50 S Central Campus Dr, Salt Lake City 84112, Utah,USA

**blair@ece.utah.edu*

Abstract: We report on the design, fabrication and optical characterization of a slow light waveguide created using a linear array of coupled resonators in a large cross-section rib waveguide. Structures with as many as 25 high aspect ratio resonators are experimentally investigated. The measured propagation loss, group velocity, and delay-bandwidth product (DBP) are presented. The metric DBP/unit loss is also introduced, with a value 38/dB. Finally we discuss a method for further reducing loss in the slow-light rib waveguide.

OCIS codes: (130.3120) Integrated optics devices; (230.5750) Resonators; (230.5298) Photonic crystals; (220.4610) Optical fabrication.

References and links

1. Y. Chen, and S. Blair, "Nonlinearity enhancement in finite coupled-resonator slow-light waveguides," Opt. Express **12**(15), 3353–3366 (2004), http://www.opticsinfobase.org/abstract.cfm?URI=OE-12-15-3353.
2. J. B. Khurgin, "Optical buffers based on slow light in electromagnetically induced transparent media and coupled resonator structures: comparative analysis," J. Opt. Soc. Am. B **22**(5), 1062–1074 (2005).
3. M. Soljačić, S. G. Johnson, S. Fan, M. Ibanescu, E. Ippen, and J. D. Joannopoulos, "Photonic-crystal slow-light enhancement of nonlinear phase sensitivity," J. Opt. Soc. Am. B **19**(9), 2052–2059 (2002).
4. Y. A. Vlasov, M. O'Boyle, H. F. Hamann, and S. J. McNab, "Active control of slow light on a chip with photonic crystal waveguides," Nature **438**(7064), 65–69 (2005).
5. B. Corcoran, C. Monat, C. Grillet, D. J. Moss, B. J. Eggleton, T. P. White, L. O'Faolain, and T. F. Krauss, "Green light emission in silicon through slow-light enhanced third-harmonic generation in photonic-crystal waveguides," Nat. Photonics **3**(4), 206–210 (2009).
6. J. F. McMillan, X. Yang, N. C. Panoiu, R. M. Osgood, and C. W. Wong, "Enhanced stimulated Raman scattering in slow-light photonic crystal waveguides," Opt. Lett. **31**(9), 1235–1237 (2006).
7. M. Ebnali-Heidari, C. Monat, C. Grillet, M. K. Moravvej-Farshi, "A proposal for enhancing four-wave mixing in slow light engineered photonic crystal waveguides and its application to optical regeneration," Opt. Express **17** 18340–18353 (2009).
8. A. Yariv, Y. Xu, R. K. Lee, and A. Scherer, "Coupled-resonator optical waveguide: a proposal and analysis," Opt. Lett. **24**(11), 711–713 (1999).
9. F. Xia, L. Sekaric, and Y. Vlasov, "Ultracompact optical buffers on a silicon chip," Nat. Photonics **1**(1), 65–71 (2007).
10. M. Notomi, E. Kuramochi, and T. Tanabe, "Large-scale arrays of ultrahigh-Q coupled nanocavities," Nat. Photonics **2**(12), 741–747 (2008).
11. T. F. Krauss, "Slow light in photonic crystal waveguides," J. Phys. D Appl. Phys. **40**(9), 2666–2670 (2007).
12. S. Hughes, L. Ramunno, J. F. Young, and J. E. Sipe, "Extrinsic optical scattering loss in photonic crystal waveguides: role of fabrication disorder and photon group velocity," Phys. Rev. Lett. **94**(3), 033903 (2005).
13. R. J. P. Engelen, D. Mori, T. Baba, and L. Kuipers, "Two regimes of slow-light losses revealed by adiabatic reduction of group velocity," Phys. Rev. Lett. **101**(10), 103901 (2008).
14. M. W. Pruessner, T. H. Stievater, and W. S. Rabinovich, "Integrated waveguide Fabry-Perot microcavities with silicon/air Bragg mirrors," Opt. Lett. **32**(5), 533–535 (2007).
15. T. F. Krauss, and R. M. De La Rue, "Optical characterization of waveguide based photonic microstructures," Appl. Phys. Lett. **68**(12), 1613–1615 (1996).
16. J. Goeckeritz, and S. Blair, "One-dimensional photonic crystal rib waveguides," J. Lightwave Technol. **25**(9), 2435–2439 (2007).
17. J. Lousteau, D. Furniss, A. B. Seddon, T. M. Benson, A. Vukovic, and P. Sewell, "The single-mode condition for silicon-on-insulator optical rib waveguides with large cross section," J. Lightwave Technol. **22**(8), 1923–1929 (2004).

#129998 - $15.00 USD Received 11 Jun 2010; revised 27 Jul 2010; accepted 3 Aug 2010; published 9 Aug 2010

18. R. A. Soref, J. Schmidtchen, and K. Petermann, "Large single-mode rib waveguides in GeSi-Si and Si-on-SiO_2," IEEE J. Quantum Electron. **27**(8), 1971–1974 (1991).
19. C. Jamois, R. B. Wehrspohn, L. C. Andreani, C. Hermann, O. Hess, and U. Gosele, "Silicon-based two-dimensional photonic crystal waveguides," Photonics Nanostruct. Fundam.Appl. **1**(1), 1–13 (2003).
20. Y. Qian, J. Song, S. Kim, and G. P. Nordin, "Compact 90 ° trench-based splitter for silicon-on-insulator rib waveguides," Opt. Express **15**(25), 16712–16718 (2007), http://www.opticsinfobase.org/abstract.cfm?uri=IPNRA-2007-IMC3.
21. U. Fischer, T. Zinke, J.-R. Kropp, F. Arndt, and K. Petermann, "0.1dB/cm waveguide losses in single-mode SOI rib waveguides," IEEE Photon. Technol. Lett. **8**(5), 647–648 (1996).
22. S. Chakraborty, D. G. Hasko, and R. J. Mears, "Aperiodic lattices in a high refractive index contrast system for photonic bandgap engineering," Microelectron. Eng. **73–74**, 392–396 (2004).
23. A. S. Jugessur, P. Pottier, and R. M. De La Rue, "Engineering the filter response of photonic crystal microcavity filters," Opt. Express **12**(7), 1304–1312 (2004), http://www.opticsinfobase.org/abstract.cfm?URI=oe-12-7-1304.
24. S. J. Wind, P. D. Greber, and H. Rothuizen, "Accuracy and efficiency in electron beam proximity effect correction," J. Vac. Sci. Technol. B **16**(6), 3262–3268 (1998).
25. X. Letartre, C. Seassal, C. Grillet, P. Rojo-Romeo, P. Viktorovitch, M. Le Vassor d'Yerville, D. Cassagne, and C. Jouanin, "Group velocity and propagation losses measurement in a single-line photonic-crystal waveguide on InP membranes," Appl. Phys. Lett. **79**(15), 2312–2314 (2001).
26. K. Kiyota, T. Kise, N. Yokouchi, T. Ide, and T. Baba, "Various low group velocity effects in photonic crystal line defect waveguides and their demonstration by laser oscillation," Appl. Phys. Lett. **88**(20), 201904 (2006).
27. M. Notomi, K. Yamada, A. Shinya, J. Takahashi, C. Takahashi, and I. Yokohama, "Extremely large group-velocity dispersion of line-defect waveguides in photonic crystal slabs," Phys. Rev. Lett. **87**(25), 253902 (2001).
28. J. Jágerská, N. Le Thomas, V. Zabelin, R. Houdré, W. Bogaerts, P. Dumon, and R. Baets, "Experimental observation of slow mode dispersion in photonic crystal coupled-cavity waveguides," Opt. Lett. **34**(3), 359–361 (2009).
29. J. Li, T. P. White, L. O'Faolain, A. Gomez-Iglesias, and T. F. Krauss, "Systematic design of flat band slow light in photonic crystal waveguides," Opt. Express **16**(9), 6227–6232 (2008), http://www.opticsinfobase.org/oe/abstract.cfm?uri=oe-16-9-6227.
30. L. H. Frandsen, A. V. Lavrinenko, J. Fage-Pedersen, and P. I. Borel, "Photonic crystal waveguides with semi-slow light and tailored dispersion properties," Opt. Express **14**(20), 9444–9450 (2006), http://www.opticsinfobase.org/oe/abstract.cfm?uri=oe-14-20-9444.
31. M. D. Settle, R. J. P. Engelen, M. Salib, A. Michaeli, L. Kuipers, and T. F. Krauss, "Flatband slow light in photonic crystals featuring spatial pulse compression and terahertz bandwidth," Opt. Express **15**(1), 219–226 (2007), http://www.opticsinfobase.org/oe/abstract.cfm?uri=oe-15-1-219.
32. T. Baba, T. Kawaaski, H. Sasaki, J. Adachi, and D. Mori, "Large delay-bandwidth product and tuning of slow light pulse in photonic crystal coupled waveguide," Opt. Express **16**(12), 9245–9253 (2008), http://www.opticsinfobase.org/oe/abstract.cfm?uri=oe-16-12-9245.

1. Introduction

Slow light using dielectric waveguide engineering has progressed rapidly in recent years. Researchers have used slow light to create wavelength-selective filters, reduce the size and power consumption of optical devices, and construct time delay lines [1–3]. Slow light has also been shown to intensify light-matter interaction and thereby enhance nonlinear effects. Accordingly, slow-light waveguides have been shown computationally and experimentally to improve nonlinear phase sensitivity, third-harmonic generation, Raman scattering, and four-wave mixing [3–7].

One method for creating chipbased slow light is through coupled resonator optical waveguides (CROWs). These structures consist of a linear array of weakly coupled resonators (e.g. microdisc, ring, Fabry-Perot or photonic crystal resonators) [8–10]. Provided there is mode overlap between adjacent resonators, light will tunnel from one resonator to the next along the array. CROWs have been used to delay light propagation for hundreds of picoseconds and reduce the group velocity v_g by a factor of several hundred [9,10]. However, these structures often exhibit large propagation losses. This is a significant problem when designing slow light waveguides, as research has shown loss to scale proportionally, or perhaps quadratically, with the slow-down factor [11–13]. Consequently, any gains from using slow light will be negated by higher losses unless proper attention is given to reducing the losses.

In this paper we investigate a CROW created using an array of resonators in a large cross-section rib waveguide. Previous work has shown that a single Fabry-Perot (FP) cavity within a

#129998 - $15.00 USD Received 11 Jun 2010; revised 27 Jul 2010; accepted 3 Aug 2010; published 9 Aug 2010

rib waveguide can be a low loss resonator [14]. This property is due to the relatively large size of the waveguide mode compared to the narrow trenches, which reduces diffraction-induced out-of-plane scattering loss [15]. In fact, the amount of loss scales inversely with the waveguide height [16]. The loss reduction, as a result, is only limited by the depth to which the high aspect-ratio trenches can be etched. Here, we extend this structure to include coupled resonators and experimentally investigate the structure's optical properties. We believe this is the first time large cross-section rib waveguides with coupled resonators have been explored from the perspective of creating slow light.

2. Waveguide design

The slow-light waveguide can be seen in Fig. 1. The waveguide is designed using a silicon-on-insulator (SOI) wafer with a Si device layer of 4.5 μm and a buried oxide layer of 2 μm. The rib width to total height ratio (*w*/H) is 0.83 and the slab height to total height ratio (h/H) is

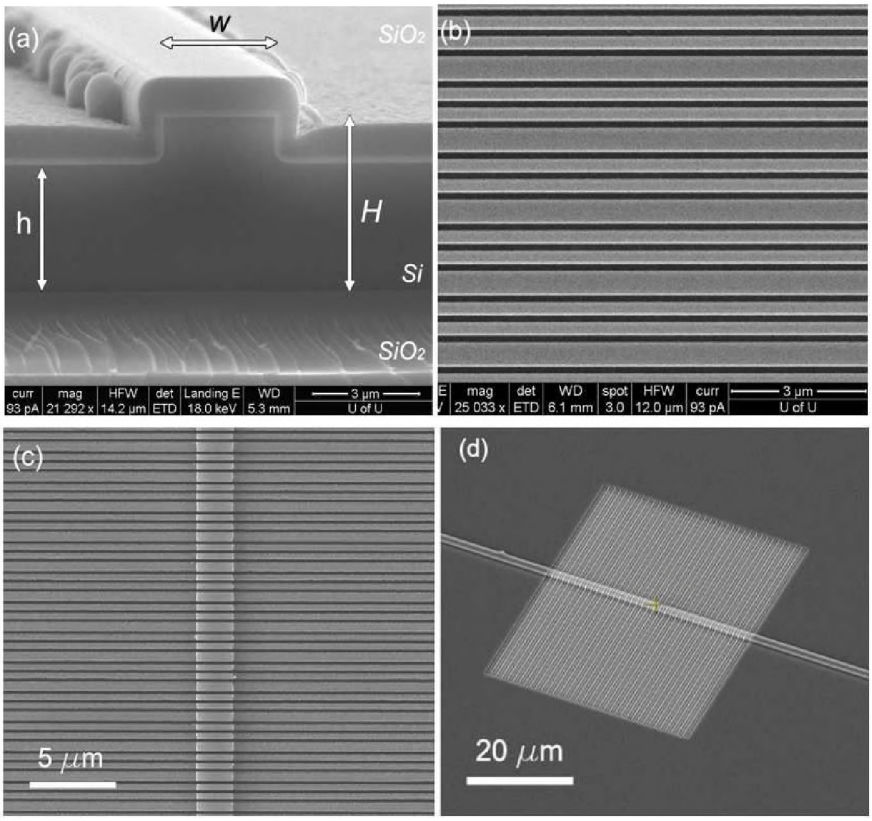

Fig. 1. Micrographs of the slow light waveguide. a) Cross section of a rib waveguide showing the top and bottom SiO_2 claddings. The rib waveguide has a height of *H*, a rib width of *w* and a slab height of *h*. b) A magnified view of the surface of the high aspect ratio trenches. Three trenches are used to separate each resonator. c) The trenches shown are etched through the rib waveguide. d) A structure with 25 coupled resonators. The input and output rib waveguide can be seen leading to the CROW.

0.66. These ratios provide a single mode at the operating wavelength, i.e. 1550 nm [17]. Single mode operation is verified with TE polarized light (electric field parallel to the slab) using the beam propagation method (BPM) (BeamProp, Rsoft Inc.). Even though the refractive index contrast between the waveguide core and cladding is large, only one mode will propagate because the effective index under the rib is higher than the effective index of the fundamental mode of the slab region [18].

#129998 - $15.00 USD Received 11 Jun 2010; revised 27 Jul 2010; accepted 3 Aug 2010; published 9 Aug 2010

The resonators are created by etching trenches down to the buried oxide. The trenches form high index-contrast distributed Bragg reflectors (DBRs). The length of the trenches in the transverse direction is $15w$. Using BPM simulations, the size of the mode in the waveguide is found to be approximately $6w$. Therefore the trench length is chosen to be much greater than this minimum length to prevent light from escaping in the transverse direction. The trenches are back filled with SiO_2 and the top cladding is also SiO_2. The top oxide makes the structure more symmetric which has been shown to reduce loss [19]. In addition, the top and bottom claddings give the structure more mechanical strength compared to other waveguides such as PC membranes. Each resonator is separated by three trenches. The width of the trenches t and the width of the spaces between trenches s are chosen so that their summation is a half-wavelength multiple. In other words, the structure is designed using the condition, $m(\lambda/2) = n_{eff}\, s + n_{sio2}\, t$, where $m = 1,2,3\ldots$, n_{eff} (3.44) is the effective index of the rib waveguide and n_{sio2} (1.45) is the index of SiO_2. The effective index is also found from the BPM simulations. To alleviate the fabrication complexity, we select $m = 2$. Accordingly, the trenches are a quarter-wavelength, $\lambda/4n_{sio2}$ and the spaces between trenches are three-quarter wavelengths, $3\lambda/4n_{eff}$. The resonator size is $3\lambda/2n_{eff}$.

3. Waveguide fabrication

The slow-light waveguides are fabricated on a 100 mm SOI wafer using a series of surface micromachining processes. The flow diagram for the fabrication is shown in Fig. 2. The first fabrication step is to perform optical lithography to create alignment marks for the trenches and waveguides. The alignment marks are etched into the wafer using reactive ion etching (RIE) with SF_6 and O_2 gases. Next, a thin layer of Cr is sputtered over the wafer followed by a spin-on layer of resist (ZEP 520A, Zeon Corp.). The resist is patterned using e-beam lithography (NovaNano, FEI) and then developed. The pattern is transferred to the Cr using RIE with Cl_2 gas. The Si is then patterned using cryogenic deep reactive ion etching (DRIE) using SF_6 and O_2 gases. The etch recipe gives smooth vertical sidewalls. The residual Cr mask is removed using wet etching (Cr-14 etchant).

Next, the rib waveguide is formed over the trenches using optical lithography and another DRIE step. This etching step uses a much higher pressure than the previous DRIE step to create a short mean free path between reactive gas molecules which prevents etching at the bottom of the trenches. The waveguide must be aligned perpendicularly to the trenches to avoid deflecting light out of the waveguide. The alignment is better than a half degree from 90°, similar to state-of-the-art fabrication quality achieved by others [20].

The trenches are back filled by wet oxidation. The wet oxidation is self-arresting as the oxide from both sides of the trenches meet. The purpose of the oxidation is to reduce surface roughness inside the trenches which lowers the waveguide loss [21]. Roughness scattering is particularly detrimental to slow light waveguides because the scattering loss scales with the square of the electric field [11].

Note that for each micron of SiO_2 grown, 0.44 μm of Si is consumed. Accordingly the trenches were designed to be narrower than the final desired size and the spaces and resonators were designed to be wider. The final trench width t_f is given by the summation, $t_f = t_i \sum 0.44^p$ where $p = 0,1,2,3\ldots$ and t_i is the initial trench width. Since t_f is designed to be a

#129998 - $15.00 USD Received 11 Jun 2010; revised 27 Jul 2010; accepted 3 Aug 2010; published 9 Aug 2010

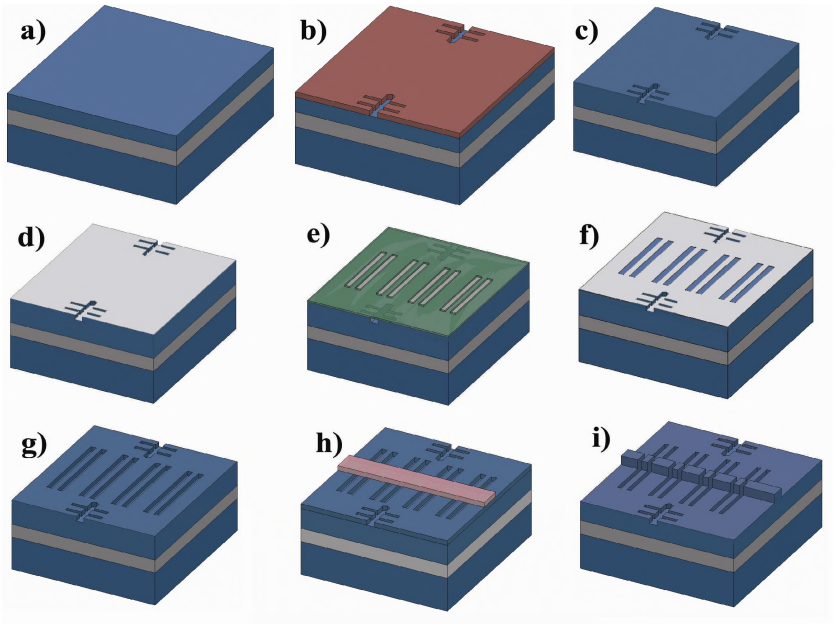

Fig. 2. Process steps used to fabricate the waveguides. a) An SOI wafer is processed starting with b) an optical lithography step using a positive photoresist (Shipley 1813) and c) dry etching using RIE. d) A layer of Cr is sputtered on the wafer surface followed by e) a spin-on layer of e-beam resist. The resist is then patterned and f) the Cr is etched using RIE. The Cr mask is then used as a mask during g) etching of the trenches. h) Another optical lithography step is used to create an etch mask for the rib waveguide, which is i) etched using a short DRIE step.

quarter-wavelength, we can solve this equation for the initial trench width. To find the initial spacing s_i between trenches and the initial resonator size before oxidation, we use the fact that the pitch Λ is the same before and after oxidation. The pitch is given by, $\Lambda = t_f + s_f = t_i + s_i$, where s_f is the spacing between trenches after oxidation. Thus, the equation for pitch can be used to solve for s_i. Note that the difference between s_i and s_f is the amount of Si consumed during oxidation. The initial resonator size R_i must be larger than the final resonator size R_f by this amount. The trenches, before and after oxidation, can be seen in Fig. 3.

A top layer of SiO_2, approximately 1.5 µm thick, is deposited on top of the structure using plasma-enhanced chemical vapor deposition (PECVD). Finally the waveguides are diced into chips and the endfaces are polished using chemical-mechanical planarization.

4. Experimental measurements

A tunable laser source (Agilent 81680A) is endfire coupled to the waveguides using a polarization maintaining lensed fiber. The tunable range of the laser is 1456 to 1584 nm, adjustable by increments of 10 pm. The fiber spot size is 3 µm (1/e beam waist). The fiber also has an anti-reflection coating to reduce back reflections. The light is polarized parallel to the waveguide slab (TE). The lensed fiber is positioned using a six-axis stage with piezoelectric controllers on the x-, y-, and z- axis. The chip sits on a three-axis stage. On the opposite side of the chip, light is collected using an identical lensed fiber. The collector fiber is also positioned with a six-axis stage. The collected light is carried to an InGaAs photodetector (Agilent 81635A). A computer then records the output power and wavelength. Above the chip is a 10x objective lens with a CCD camera mounted to a custom-built three-axis stage. The camera is used to visually align the fibers and the chip.

#129998 - $15.00 USD Received 11 Jun 2010; revised 27 Jul 2010; accepted 3 Aug 2010; published 9 Aug 2010

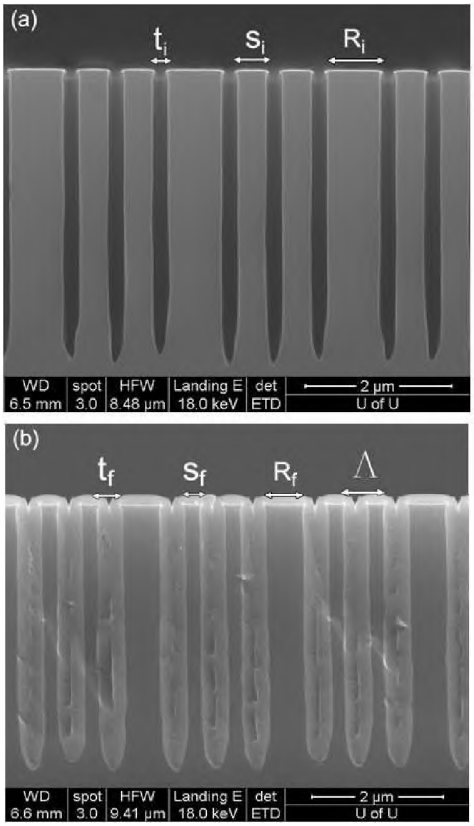

Fig. 3. High aspect ratio trenches etched into a) the silicon device layer and b) back filled via wet oxidation. At the center of the trenches in b), an interface boundary can be seen where the oxide growth meets. The boundary is estimated to be less than 5 nm. Note the difference between t_i and t_f is equal to the amount of Si consumed during oxidation.

5. Optical characterization

5.1 Loss measurements

There are ten rib waveguides on each chip. The propagation loss coefficients of the rib waveguides are found by performing a spectral transmission measurement and using the FP technique [22]. The average loss is 4.0 ± 0.8 db/cm. The average insertion loss for the waveguides is 13.2 dB. A larger fiber spot size would have reduced the insertion loss.

The loss of the CROWs is measured using a modification of the cutback method. The output power of a waveguide can be described by the relationship $P_{out} = P_{in}\exp(-\alpha L)$ where P_{out} and P_{in} are the output and input power respectively, L is the length of the waveguide and α is the loss coefficient. The loss coefficient is found by taking the ratio of two power measurements of waveguides with different lengths and solving for α, thus, coupling losses are factored out. The CROWs on our chips are 10.8, 21.6 and 54.1 µm long for waveguides with 5, 10, and 25 resonators respectively; thus, the chip does not need to be cut to obtain different waveguide lengths. Since the waveguides are not cut, errors that could occur in the measurements from variations in endface polishing are eliminated. Note that the rib waveguides leading to and from the CROWs are different lengths, but knowing these lengths and the loss coefficient found previously for the unpatterned rib waveguides allows us to remove the differential loss contribution. Nine CROWs are measured on each chip. The average loss is 53 ± 7dB/cm at λ = 1560 nm.

#129998 - $15.00 USD Received 11 Jun 2010; revised 27 Jul 2010; accepted 3 Aug 2010; published 9 Aug 2010

5.2 Group velocity measurements

The measured transmission spectra for three CROWs with 5, 10 and 25 resonators are shown in Fig. 4. The CW input power is 1mW. The plots have been normalized by the fiber to fiber transmission (note that this is an arbitrary normalization which does not affect the cutback loss calculations). The left edge of the bandgap is at approximately 1480 nm and the resonant passband is centered at 1565 nm. The right edge of the bandgap is outside the wavelength range of the tunable laser source. For each resonator in the waveguide there is a miniband transmission peak. This can be seen most easily in Fig. 4a where 5 resonant peaks are easily discernable. The peaks, however, are wider and shallower than expected. This anomaly is due to stronger than anticipated coupling between the CROW and the input and output waveguides. The stronger coupling occurs because the outermost trench in the CROW is narrower than the other trenches. During fabrication the trenches are first defined by e-beam lithography. When the e-beam writes over the resist, the outermost trench does not receive cross exposure on both sides. As a result of this proximity effect the trench is narrower. This

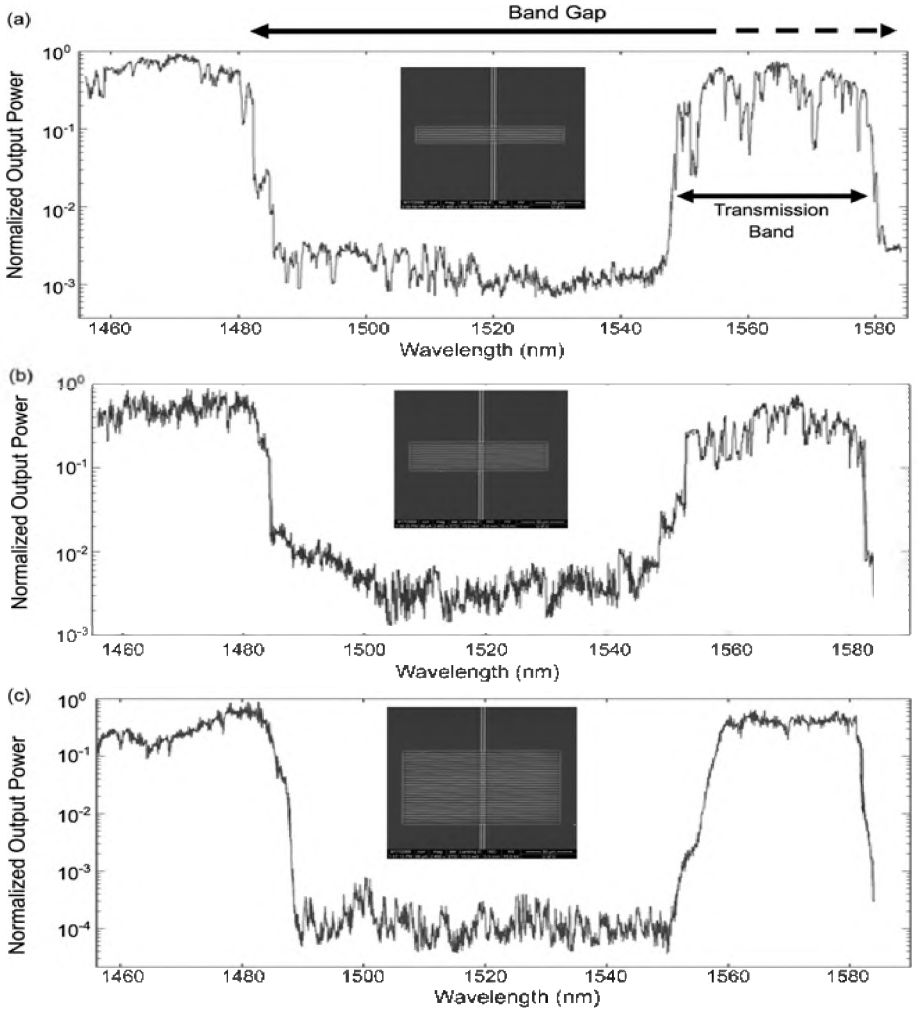

Fig. 4. Normalized transmission spectra for the slow light rib waveguides with a) 5, b) 10, and c) 25 resonators. The inset in each plot shows a micrograph of the corresponding structure.

#129998 - $15.00 USD Received 11 Jun 2010; revised 27 Jul 2010; accepted 3 Aug 2010; published 9 Aug 2010

leads to stronger coupling between the CROW and rib waveguide which has been shown to smooth the transmission spectra and widen resonances [23]. (Note there are numerous methods that can be used to counter the proximity effect, for example see [24].) The resonances may also be smoother because of small structural disorder on the waveguide surface, which can be seen in Fig. 1c.

Based on the FP condition for resonance, the group velocity can be calculated from the spacing of the resonant peaks in the spectral transmission plots [25–28]. Figure 5 shows a close-up plot of the measured output power for a structure with 25 resonators. The transmission spectrum is a composite of the interference patterns from three waveguides: the unpatterned input and output rib waveguides and the CROW. The narrowly spaced resonances are from the rib waveguides and the widely spaced ones are from the CROW.

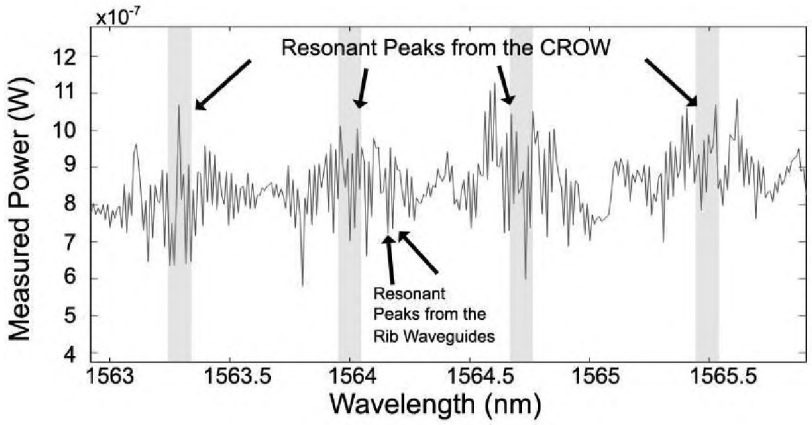

Fig. 5. A close-up plot of the output power for the CROW with 25 resonators. The fringes are caused by the FP cavities formed by the input rib waveguide, CROW, and output rib waveguide. A beating pattern can be seen due to the rib waveguides which are similar in length.

The group velocity can be calculated from $v_g = (2cL\Delta\lambda)/(\lambda_1\lambda_2)$, where λ_1 and λ_2 are adjacent fringe peaks and $\Delta\lambda$ is the spacing between peaks. The group index can easily be obtained from this equation. The average n_g is 29 (averaged over three 25 resonator CROWs). The group index is calculated at the center of the passband, where the minimum slowing occurs. The group indices of the 5 and 10 resonator structures are slightly higher at 36 and 33 respectively, again averaged over three structures each. The group index is not the same for all structures most likely because of slight differences in coupling strengths between the CROWs and the input/output rib waveguides (i.e. different impedance matching). The 25 resonator CROWs are most strongly coupled to the rib waveguide followed by the 10 and 5 resonator structures. This variation in coupling also explains why the 25 resonator and 10 resonator structures have shallower oscillations in their transmission spectra with the oscillations decreasing for stronger coupling to the rib waveguide.

The excellent capability of the rib waveguide CROW to reduce v_g is due to a high index contrast. Large cross-section rib waveguides have effective indices close to the index of the guiding material. In our case, the effective index found from BPM simulation is 3.44, creating an index contrast along the optical axis of approximately 2. For comparison, a PC W1 using the same materials has an effective index of 2.7. Assuming air holes are used in the PC, the index contrast is only 1.7.

Figure 6 shows the variation in the group index with wavelength for a 25 resonator structure. The circle symbols represent the group index values calculated from measurements and the solid line is a fit using the theoretical equation for the group index of an

#129998 - $15.00 USD Received 11 Jun 2010; revised 27 Jul 2010; accepted 3 Aug 2010; published 9 Aug 2010

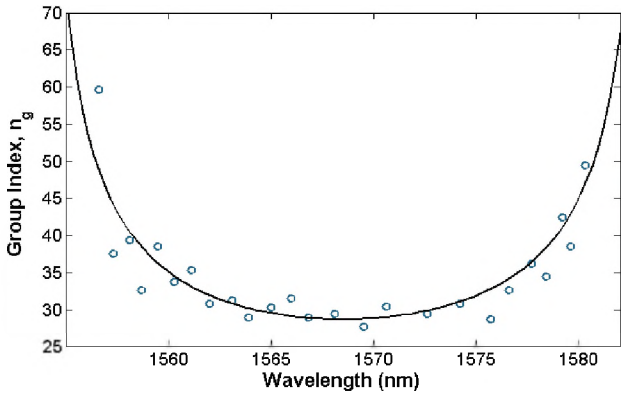

Fig. 6. The wavelength dependence of the group index calculated for a 25 resonator structure. The open circle points are the values of n_g calculated from measurements and the solid line is a fit-line for an infinite structure.

infinite structure [1]. Even though the structure has a relatively smooth transmission band, the group index is still parabolic in shape, with oscillations due to the discrete resonators. At the center of the band (approximately 1561 to 1577nm), the group index varies by ± 10% about an average value of 30.1.

5.3 Delay-bandwidth product

For slow light waveguides to be used in all-optical networks as time-delay buffers, they must be capable of significantly reducing the group velocity. In addition, they must also have a wide bandwidth to accommodate optical signals and avoid pulse distortion. Therefore, the delay-bandwidth product (DBP) is an important figure of merit. For the 25 resonator waveguide, the bandwidth over which n_g varies by ± 10% about the average n_g is 16 nm. This bandwidth was found using the fit line in Fig. 6. We refer to this as the smooth n_g bandwidth [29]. The calculated delay time is 5.4 ps, giving a DBP of 10.8. This is a relatively large value and compares well to state-of-the-art slow light waveguides (see Table 1). Note, in Table 1, the structures studied by Frandsen and Li are low-dispersion devices and therefore have additional constraints imposed on the design.

The DBP could be increased by coupling more resonators together. However, as more cavities are added, loss also increases, limiting the practical length. Therefore another important figure of merit is the DBP per unit loss. For our structure with 25 resonators the DBP/loss is 38 per dB, which is also shown in Table 1 along with the values for several other slow light waveguides from the literature. On a DBP/loss basis, the waveguide presented here has the second best performance.

The normalized DBP (nDBP) is also an important figure of merit for comparing the performance of various waveguides. The nDBP is defined as $n_g(\Delta\omega/\omega)$ where ω is the frequency and $\Delta\omega$ is the bandwidth. For the structure presented here, the value is 0.31, which compares favorably to other slow light structures [29].

6. Discussion and conclusion

The large cross section CROW exhibits a promising combination of low loss, slow group velocity, and wide bandwidth. The loss, moreover, could be further reduced by increasing the waveguide height, H, and thereby further reducing out-of-plane scattering loss. The limiting factor for fabricating a thicker waveguide is etching the high aspect ratio trenches. Our fabrication procedure can be used to construct $\lambda/4$ trenches approximately 8 μm deep. Based on the FDTD simulations from our previous work, we estimate this structure would exhibit nearly three orders of magnitude lower out-of-plane scattering loss (see Fig. 4 in ref. 16).

#129998 - $15.00 USD Received 11 Jun 2010; revised 27 Jul 2010; accepted 3 Aug 2010; published 9 Aug 2010

Table 1. Comparison of slow light waveguides from the literature.

Structure	Measurement Type	Group Index	DBP	Propagation Loss (dB/cm)	DBP/loss (dB^{-1})	Reference
1. Coupled Rib Waveguide Resonators[a]	Spectral	30.1	10.8	52.7	38.0	Presented Here
2. Coupled PC Resonators	Temporal and Spectral	129	11.0[b]	14.5[c]	39.9	Notomi [10]
3. Coupled PC Resonators	Spectral	105	3.0[d]	$3x10^3$	0.4	Jágerská [28]
4. Coupled Ring Resonators	Temporal and Spectral	36.3[e]	55[e]	126[e]	2.4	Xia [9]
5. PC Band Edge	Spectral	34	78[f]	150	10.4	Frandsen [30]
6. PC Band Edge	Spectral	25	30	244	7.7	Settle [31]
7. PC Band Edge	Spectral	42	57	-	-	Baba [32]
8. PC Band Edge	Spectral	44	15.8[d]	-	-	Li [29]

[a] Measured for a 25 resonator structure with the n_g spectrum shown in Fig. 6.
[b] Calculated using bandwidth of 1.2 nm, N = 60 resonators, $v_g = 7.7x10^{-3}c$, and 75 ps delay time.
[c] Estimated loss.
[d] Calculated from paper.
[e] Calculated for 100 coupled rings in CROW configuration, i.e. 9 μm radii and 200 nm gap. The linear length is used to calculate the propagation loss and group index, not the total path length. A 2 nm bandwidth centered at 1550 nm is used to calculate DBP.
[f] Calculated with 11 nm bandwidth, i.e. bandwidth over which n_g is reported to be constant.

However, the overall loss is a combination of several factors such as surface roughness, scattering, absorption, and structural disorder. Therefore, for a taller waveguide, one would expect the total loss to be primarily a function of these sources.

The CROW presented here is also promising because of the ease of coupling light into the waveguide. For many Si channel and PC waveguides, coupling requires adiabatic tapers or mode size converters which complicate the fabrication process. For the large cross section CROW, finding the center of the waveguide and coupling light into it using a fiber optic translation stage is simple because of the large mode size. As a result, injecting light into our waveguide is straightforward.

Despite the relatively large height of the rib waveguide, the overall footprint is still quite small. The 25 resonator CROW as fabricated occupies a surface area of approximately $3x10^{-3}$ mm^2 which is nearly half the footprint of 25 coupled ring resonators, assuming 8 μm radii and 200 nm gaps. The rib waveguide CROW footprint could be reduced further by shortening the length of the trenches. As mentioned, our BPM simulations show that the trenches only need to be 6 times the waveguide's rib width *w*. Therefore, the footprint of the 25 resonator structure could be reduced to $1.4x10^{-3}$ mm^2. This compact footprint makes the rib waveguide CROW promising for on-chip integration with other optical structures.

Acknowledgements

This work was supported by the United States Army Research Office (USARO) under grant W911NF-07-1-0245. In addition, some of the fabrication steps were performed at the Stanford Nanofabrication Facility of NNIN supported by the National Science Foundation (NSF) under Grant ECS-9731293. One author thanks M. W. Pruessner, N. Latta, and J. Conway for their advice regarding fabrication.

#129998 - $15.00 USD Received 11 Jun 2010; revised 27 Jul 2010; accepted 3 Aug 2010; published 9 Aug 2010